

1 **Observation-based estimate of Earth’s effective radiative forcing**

2 Senne Van Loon*, Maria Rugenstein, and Elizabeth A. Barnes

3 *Department of Atmospheric Science, Colorado State University, Fort Collins, Colorado, USA*

4 **Corresponding author:* Senne Van Loon; 970-491-8682; senne.van_loon@colostate.edu;

5 Colorado State University, Department of Atmospheric Science,

6 200 West Lake Street, 1371 Campus Delivery, Fort Collins, CO 80523-1371

7 The authors have no competing interests to declare.

8
9 *Classification:* Physical Sciences; Earth, Atmospheric, and Planetary Sciences

10 *Keywords:* Radiative forcing, Energy budget, Climate

13 **Human emissions continue to influence Earth’s climate. Effective radiative forcing quantifies**
14 **the effect of such anthropogenic emissions together with natural factors on Earth’s energy**
15 **balance (Soden et al. 2018; Gregory et al. 2020; Forster et al. 2021, 2024). Evaluating**
16 **the exact rate of effective radiative forcing is challenging, because it can not be directly**
17 **observed. Therefore, estimating the effective forcing usually relies heavily on climate models**
18 **(Forster et al. 2024). Here, we present an estimate of effective radiative forcing that makes**
19 **optimal use of observations. We use artificial intelligence to learn the relationship between**
20 **surface temperature and radiation caused by internal variability in a multi-model ensemble.**
21 **Combining this with observations of surface temperature and the Earth’s net radiative**
22 **imbalance (Loeb et al. 2018, 2021; NASA/LARC/SD/ASDC 2023), we predict an effective**
23 **forcing trend of $0.72 \pm 0.20 \text{ Wm}^{-2}$ per decade for 2001-2023. Our method enables a new and**
24 **independent assessment of the observed effective radiative forcing since 1985, that can be**
25 **updated simultaneously with available observations. We make advances to close the Earth’s**
26 **energy budget on annual timescales, separating the influence of forcing versus the radiative**
27 **response to surface temperature variations. Effective radiative forcing has substantially**
28 **increased since 2021 and has not been countered by a strongly negative radiative response,**
29 **consistent with an exceptionally warm year of 2023 and 2024.**

30

31 *Significance Statement:* Effective radiative forcing is the radiative perturbation of the atmo-
32 sphere due to, e.g., emissions, before surface temperature changes. Quantifying this effect is
33 key to understanding Earth’s energy balance, testing climate theories, building climate models,
34 and attributing climate change. Effective forcing cannot be observed and its calculation relies
35 on climate models, which come with biases and assumptions of emissions and cloud processes
36 that are not understood well yet. Here, we develop a new framework to calculate historical
37 forcing that makes minimal use of climate models, by combining artificial intelligence with direct
38 observations. Our forcing estimate indicates a strong upwards trend in the last two decades, can
39 be updated immediately with new observations, and increases our understanding of Earth’s recent
40 energy imbalance.

41 Effective radiative forcing (F) and the radiative response to forcing (R , hereafter referred to as ra-
42 diation) simultaneously modify the radiation budget of the Earth (N). The simplest energy balance
43 model states that, globally averaged,

$$N = F + R. \quad (1)$$

44 Only N can be measured by satellites recording the energy flux in and out of the entire Earth
45 system (Loeb et al. 2018, 2021; NASA/LARC/SD/ASDC 2023). A positive effective forcing F
46 (excess energy introduced into the atmosphere) is generally balanced by a negative response R , but
47 both are time-varying. In a stable climate, R balances F . A positive N indicates excess energy
48 storage in the Earth system.

49 Effective radiative forcing (hereafter “forcing” F) is the sum of instantaneous radiative forcing
50 (initial flux changes after a perturbation in emissions or prescribed concentrations in greenhouse
51 gases or aerosols) and radiative adjustments (radiative flux changes induced by the forcing within
52 the atmosphere but independent of surface temperature; e.g., Sherwood et al. 2015; Smith et al.
53 2020; Forster et al. 2021; Sherwood et al. 2020). Instantaneous radiative forcing has recently been
54 estimated from observations using radiative kernels (Kramer et al. 2021), but radiative adjustments
55 have to be added to make its use valid in equation (1) and to compare it to other estimates of radiative
56 forcing (see discussion below; Forster et al. 2024). Radiative adjustments rely on climate models
57 and are very uncertain. Here, we directly estimate effective radiative forcing without relying on the
58 concept of radiative adjustments or climate models calculating them.

59 Estimates of historical forcing are uncertain because it requires the input of external factors such
60 as greenhouse gas concentrations or aerosol emissions and relies on specific implementations of
61 parametrizations that can lead to model biases (Soden et al. 2018; Bellouin et al. 2020; Forster
62 et al. 2021, 2024). Here, we present a new method to quantify effective radiative forcing from the
63 observed surface temperature and radiative imbalance, using a minimal number of assumptions.
64 We combine observations with physically explainable machine learning methods to predict the
65 radiative response to surface warming, from which we subsequently estimate the historical radiative
66 forcing.

1. Convolutional neural network predicts radiative response

The radiation R is an aggregate of many processes initiated by the perturbation of a forcing. For example, CO_2 or aerosols change the structure of temperature in the atmosphere and at the surface, and the amount and distribution of water vapour, clouds, snow, sea ice, and vegetation. In turn, all of these factors can change the radiation balance of the Earth, both in the net shortwave solar radiation and the longwave outgoing radiation (Charney et al. 1979; Cess et al. 1990; Roe 2009). Research over the last decade has highlighted that global-mean radiation sensitively depends on the spatial patterns of surface warming, termed the pattern effect (Senior and Mitchell 2000; Andrews et al. 2015; Rugenstein et al. 2023).

We predict R from maps of surface temperature (T) with a convolutional neural network (CNN; Supporting Information Fig. 1 and Methods). CNNs have recently gained popularity in the geosciences (Reichstein et al. 2019), because they are well-equipped to recognize nonlinear spatial patterns in images (LeCun et al. 2015). It has been shown that CNNs outperform traditional and regularized linear methods in predicting global-mean radiation from spatial variations of T caused by internal variability (Rugenstein et al. in review). Here, we train a CNN to recognize the relationship between maps of T and the globally averaged R caused by internal variability in large initial condition ensembles of four climate models (see Methods). That is, the forced response is removed from all data prior to training by subtracting the ensemble mean, leaving only natural variations in T and R .

Training on internal variability removes the need to rely on the correct simulation of forcing or forced surface warming in climate models. We only make the assumption that climate models correctly simulate the relationship between the spatial pattern of T and global-mean R in an unperturbed climate. We do not argue that any individual model is fully correct (Forster et al. 2021; Maher et al. 2023; Myers et al. 2021), but rely on the spread and diversity in the multi-model ensemble to be broad enough to lie *around* the true relationship between T and R (Olonscheck and Rugenstein 2024).

The CNN replaces the usual approximation that R is linearly dependent on global-mean temperature (Gregory et al. 2004; Sherwood et al. 2020), which is unable to explain large variations of radiation in the historical record (Andrews et al. 2015; Gregory et al. 2020; Rugenstein et al. 2023). Instead, the CNN takes into account the spatial pattern effect, along with potential nonlin-

97 earities among T and R . The CNN successfully reproduces held-back testing members with high
98 skill (Supporting Information Fig. 3a-b). Moreover, CNNs trained on data from only three models
99 can effectively predict R in the fourth model, indicating that our CNN can make out-of-sample pre-
100 dictions. Importantly, the CNN skilfully predicts the forced response to temperature patterns that
101 have seen strong radiative forcing (Supporting Information Fig. 3c-d). That is, applying the CNN
102 to simulated temperature maps from a warming climate (as opposed to the internal variability the
103 CNN is trained on), we correctly predict a negative trend in R . This is evidence that the CNN is
104 transferable to real-world climate change.

105 2. Quantifying observed radiative forcing

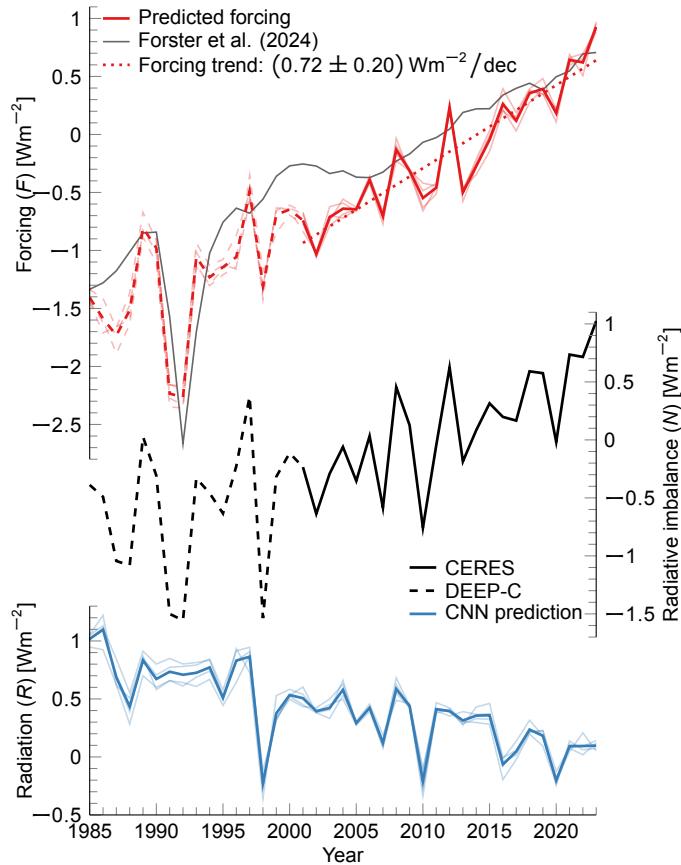
106 We estimate the historical forcing with Eq. (1) by quantifying R with our CNN, and subtracting
107 R from the observed N :

108 First, we apply observed surface warming patterns since 1985 to the CNN (Fig. 1, bottom blue
109 lines). Different observational products result in very similar radiation responses (see Methods).
110 Crucially, these observation-derived temperature maps have not been used to train the CNN, and
111 they include a forced trend. Although the CNN has not been trained on forced climate change, the
112 predicted radiation has a significant negative trend, as it should in a changing climate in which F
113 increases (Raghuraman et al. 2021; Roe 2009; Knutti and Rugenstein 2015).

119 Second, the radiative imbalance N can be derived from the satellite record (Fig. 1, middle black
120 line). Since 2001, these measurements are considered fairly precise (solid black line, derived from
121 CERES, Loeb et al. (2018)) but N has been reconstructed back to 1985 from older satellite products
122 (dashed black line, DEEP-C, Allan et al. (2014); Liu et al. (2020); Liu and Allan (2022)).

123 Finally, we quantify the forcing (Fig. 1, top red lines) by subtracting our predicted radiative
124 response from the observed imbalance (i.e., $F = N - R$). This new estimate of F primarily uses
125 observable quantities: the radiative imbalance and surface warming patterns. At the same time,
126 we limit the use of climate model input: the relationship between T and R learned from internal
127 variability only.

128 Our forcing estimate has a significant positive trend of $0.72 \pm 0.20 \text{ Wm}^{-2}\text{decade}^{-1}$ (5%-95%
129 confidence range, see Methods) in the period 2001-2023 (Fig. 1, dotted red line). This confirms
130 that the Earth system is experiencing a rapid increase in forcing. We predict a stronger trend in F

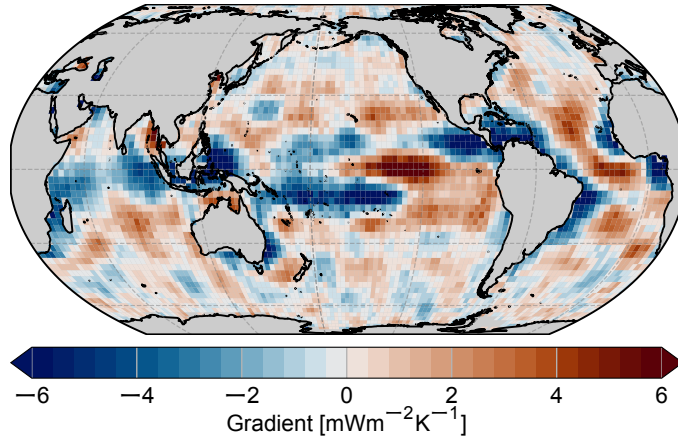


114 **Fig. 1. Radiative forcing derived from observations.** Bottom panel shows radiation (R , blue) predicted
 115 by the convolutional neural network from four observational surface temperature datasets (thin lines; thick line
 116 shows the average). Middle panel is the observed radiative imbalance (N , black). Top panel shows the predicted
 117 radiative forcing ($F = N - R$, red), and the dotted red line is the best linear fit for 2001-2023. As a comparison,
 118 the thin black line shows the radiative forcing from Forster et al. (2024).

131 than Forster et al. (2024) (top thin black line in Fig. 1, with a trend of $0.52 \text{ Wm}^{-2} \text{ decade}^{-1}$ in the
 132 same period), although it lies within the 5%-95% confidence range.

133 Contrary to other methods, we can resolve interannual variability of the forcing. For example, we
 134 correctly predict a strongly negative forcing in 1991/1992, when natural aerosol emissions peaked
 135 due to the 1991 Pinatubo eruption (Minnis et al. 1993; Stenchikov et al. 2009).

136 Over the last decade, the Earth energy imbalance has steadily increased (Hodnebrog et al. 2024;
 137 von Schuckmann et al. 2023; Storto and Yang 2024; Cheng et al. 2024) and may even be ac-
 138 celerating (Forster et al. 2024; Loeb et al. 2024b), most likely due to increased anthropogenic



149 **Fig. 2. Gradient map of the convolutional neural network.** The map shows the derivative of global mean
 150 radiation to local surface temperature, and can thus be interpreted as local radiative feedback. Gradient maps are
 151 dependent on the input, because the CNN is nonlinear. Gradients with respect to detrended temperature maps
 152 from the testing dataset are averaged.

139 forcing (Raghuraman et al. 2021; Hodnebrog et al. 2024). Our results provide independent evi-
 140 dence that this increasing N is driven by an escalating F . Based on trend analysis, F increased
 141 by $0.51 \pm 0.61 \text{ Wm}^{-2}$ from 2001 to 2010, and by $0.80 \pm 0.44 \text{ Wm}^{-2}$ from 2011 to 2020, indicating
 142 an acceleration of the forcing. This acceleration could be explained by a reversed aerosol forcing
 143 trend (Quaas et al. 2022; Kramer et al. 2021), slowing down the global cooling effect of aerosols.

144 3. Further evidence supporting our approach

145 Our method relies on the CNN to learn the correct relationship between radiation and surface
 146 temperature patterns. Although machine learning techniques are often regarded as a black box,
 147 explainable artificial intelligence (XAI) techniques (Mamalakos et al. 2022) allow us to understand
 148 why and how the CNN makes predictions.

153 Local gradients of the CNN explain the sensitivity of the CNN to local temperature variations
 154 and can be interpreted as radiative feedback arising from internal variability. Radiative feedback
 155 characterizes how radiation responds to changes in temperature through processes including clouds,
 156 sea ice, or water vapor (Roe 2009; Lutsko and Takahashi 2018; Ceppi and Nowack 2021). A local
 157 positive feedback indicates that R increases when T in that location increases. This increased
 158 incoming radiation can eventually lead to higher global temperature, hence a positive feedback.

159 Conversely, a negative feedback is stabilizing: increased temperature causes a negative response
160 R , which slows down warming of the planet.

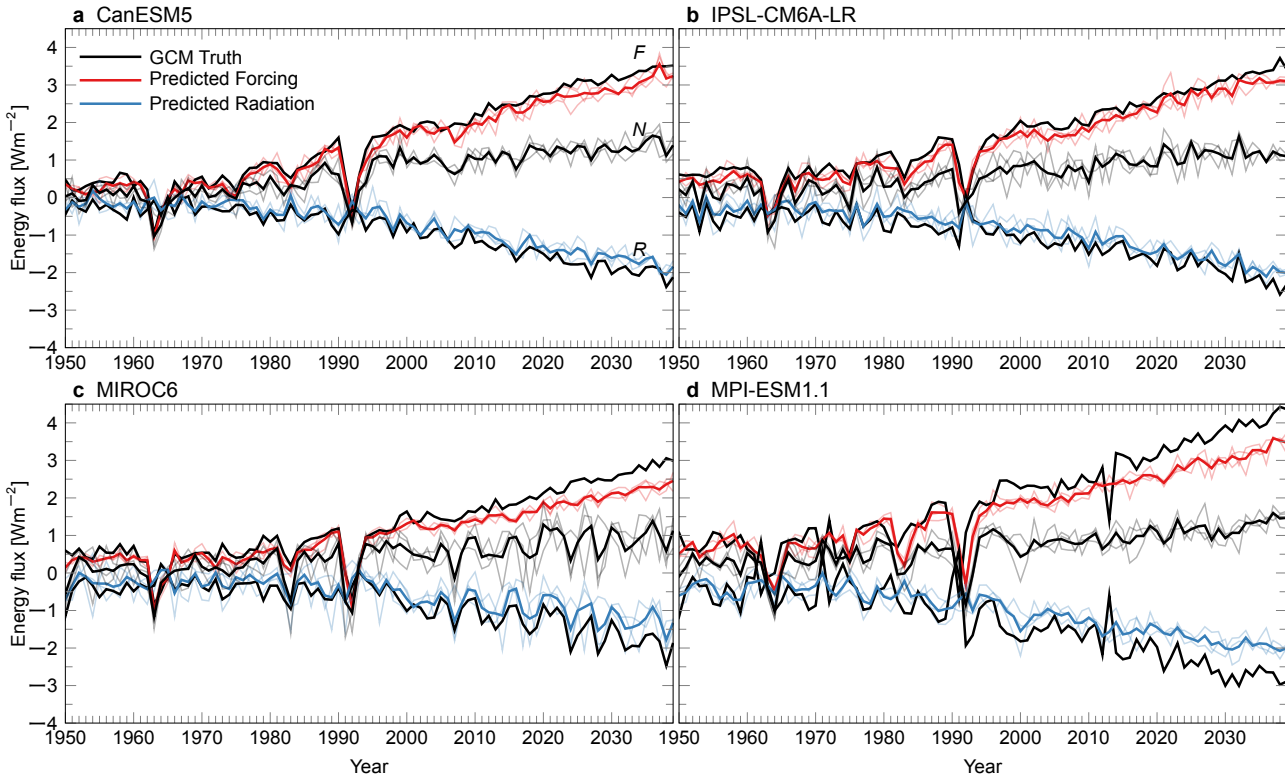
161 The gradient of the CNN (Fig. 2 and Methods) elucidates the physically meaningful regions used
162 to make predictions. For example, the large amplitude of the gradient in the Tropics reveals that the
163 CNN is most sensitive to temperature changes in these areas. Regions of tropical deep convection,
164 such as the Western Pacific, show strong negative values, interpreted as negative feedbacks. These
165 negative feedbacks are caused by changes in nonlocal lower tropospheric inversion strength, mod-
166 ulating low cloud coverage and hence radiation (Dong et al. 2019; Alessi and Rugenstein 2023;
167 Wood and Bretherton 2006). In contrast, increased temperature in more stable areas (e.g., the sub-
168 tropical Eastern Pacific) can cause a local decrease in shallow marine clouds and a positive radiative
169 response, as indicated by a strong positive feedback. Importantly, the CNN learns this relationship
170 without explicit knowledge of the underlying physical processes.

176 We further evaluate the reliability of our approach by using existing climate model simulations.
177 For the climate models used to train the CNN, designated model runs provide an estimate of F
178 (Pincus et al. 2016, Methods), while T and N are available as standard model output. Instead of
179 using observations, here we use the simulated temperature maps to predict R in the climate models
180 (Fig. 3, blue lines). Then, we subtract the simulated N (Fig. 3, middle black lines) from the result
181 to predict F (Fig. 3, red lines). For most models, the CNN is able to reproduce the simulated F
182 (Fig. 3, top black lines) almost perfectly. Note that we perform this test on ensemble members that
183 have not been used to train the CNN. For MPI-ESM, the forcing is underestimated by $\sim 20\%$ by
184 2039, due to it simulating a stronger climate scenario (RCP8.5, see methods) compared to the other
185 models (SSP2-4.5).

186 We are able to correctly predict F in the climate models, even though the CNN was trained on
187 internal variability only. This, combined with the physically meaningful gradient maps (Fig. 2),
188 increases our trust that our CNN learned a credible relationship between T and R and that our
189 estimate of historical F is trustworthy.

190 **4. Implications for past and future climate change**

191 Our approach is independent of previous assessments of the forcing. Forster et al. (2024) (Fig. 1,
192 top thin black line) finds a similar value based on a combination of model simulations and emission



171 **Fig. 3. Radiative forcing estimated and simulated by four climate models.** Radiative response (R , bottom
 172 blue lines) and radiative forcing (F , top red lines) as predicted by the convolutional neural network (CNN) com-
 173 pared to the true model output (black lines). The middle black lines are the radiative imbalance (N) from the
 174 climate model, used to predict the forcing ($F = N - R$). Thick lines indicate ensemble averages, thin lines are
 175 individual ensemble members.

193 measurements. Our trend in F is somewhat higher than previous estimates (Bellouin et al. 2020;
 194 Raghuraman et al. 2021; Hodnebrog et al. 2024; Forster et al. 2024), but lies within the 5%-95%
 195 confidence range of other methods. Most other estimates are restricted to shorter periods and do
 196 not include 2023 yet. We highlight that our method allows us to estimate F instantaneously as soon
 197 as observations of surface warming (T) and radiative imbalance (N) become available and does not
 198 rely on model intercomparison protocols, bottom-up emission estimates, or expert assessments.

199 *a. Stabilizing feedbacks*

200 By construction, our estimate of the forcing trend ($0.72 \pm 0.20 \text{ Wm}^{-2} \text{ decade}^{-1}$ for 2001-2023)
 201 is consistent with stabilizing radiative feedbacks in the last two decades. The CNN predicts a

202 trend in R of $-0.21 \pm 0.10 \text{ Wm}^{-2}\text{decade}^{-1}$. Reformulating this in terms of radiative feedbacks, i.e.
203 $\lambda = \Delta R / \Delta \bar{T}$ with $\Delta \bar{T} = 0.22 \text{ K/decade}$, we find an effective feedback parameter of $-1 \text{ Wm}^{-2}\text{K}^{-1}$.
204 Conversely, other current estimates of F imply unrealistic values of R and feedbacks. For exam-
205 ple, using the CERES observed N ($0.51 \pm 0.17 \text{ Wm}^{-2}\text{decade}^{-1}$) and estimated F by Forster et al.
206 (2024) ($0.52 \text{ Wm}^{-2}\text{decade}^{-1}$) results in an unrealistically low $\Delta R = -0.01 \text{ Wm}^{-2}\text{decade}^{-1}$, imply-
207 ing a feedback of only $-0.05 \text{ Wm}^{-2}\text{K}^{-1}$. This feedback estimate suggests that increasing global
208 temperature barely balances the excess forcing and implies that the Earth's temperature would
209 sharply increase if the feedback and forcing trend remain constant. Our estimate is more realis-
210 tic in terms of physical understanding of radiative feedbacks, which are universally recognized as
211 stabilizing in the global mean for the current climate state and all commonly used future scenarios
212 of climate change (Forster et al. 2021; Lee et al. 2021; Gregory et al. 2004, 2020; Bloch-Johnson
213 et al. 2021; Dessler and Forster 2018; Dessler 2010).

214 *b. Annually resolved drivers of the radiative imbalance*

215 Our approach gives unique insight into annual drivers of the observed radiative imbalance N .
216 According to Eq. (1), N can be influenced by F (a particular forcing) or R (response to the ob-
217 served warming patterns and radiative feedbacks). As mentioned above, the low N in 1991/1992
218 is consistent with a negative F from the eruption of Pinatubo (Minnis et al. 1993; Stenchikov et al.
219 2009), while R remained approximately constant. In contrast, in 2010, the low N occurs in con-
220 junction with an anomalously negative R , which we attribute to high anomalous temperatures in
221 the West Pacific and low temperatures in the East Pacific.

222 Since 2021, F has increased strongly (Fig. 1). This has been linked to stricter international ship-
223 ping regulations on aerosol emissions, that went into effect in 2020 (Yuan et al. 2024; Gettelman
224 et al. 2024), although this increase in forcing was counter-acted by the Hunga Tonga-Hunga Ha'apai
225 eruption in 2022 (Schoeberl et al. 2024). The rising F , in combination with a steady trend in R ,
226 contributed to an increase in the radiative imbalance in the last three years.

227 The year 2023 was exceptionally warm (Esper et al. 2024; Min 2024). The causes behind this
228 record are still unknown, and there is disagreement on whether it can be explained by internal
229 variability (Samset et al. 2024; Jiang et al. 2024; Raghuraman et al. 2024) or was due to external
230 forcing (Rantanen and Laaksonen 2024; Gettelman et al. 2024; Min 2024; Kuhlbrodt et al. 2024;

231 Schoeberl et al. 2024). According to our results, the large N in this year was mostly induced by a
232 large F . In the satellite record, the observed N has never been as high, while R did not decrease
233 enough to balance N . That is, the observed temperature pattern in 2023 did not induce a radiative
234 effect stabilizing enough to counteract the increased F . The continued amplification of the forcing,
235 together with a weak radiative response could explain the remarkably warm 2023.

236 Eq. (1) does not include the influence of natural variations on N . In principle, also the internal
237 variability of the ocean heat content affects N , independent of F and R (Raghuraman et al. 2021).
238 Therefore, we cannot exclusively attribute changes in N to F and R . However, our method allows
239 for the addition of ocean heat uptake, which could move the understanding of forcing from decadal-
240 long trends towards annual timescales.

241 *c. Outlook*

242 We use the recently demonstrated dependence of global-mean radiation on patterns of surface
243 warming (the pattern effect) to predict effective radiative forcing with a novel framework. Our
244 convolutional neural network allows us to rely on climate models less than traditional methods and
245 predict physically realistic values of R . We confirm the order of magnitude and acceleration of
246 effective forcing, but our estimate lies on the high end of former approaches. Yet, our effective
247 forcing estimate might still be too conservative, because tests in strong climate change scenarios
248 indicate that the CNN slightly underestimates the forcing (e.g., Fig. 3d).

249 Our work moves towards attribution and increased physical understanding of annual values of
250 the global-mean radiative imbalance. Combining our approach with in-situ ocean heat uptake es-
251 timates could strengthen and formalize this annual attribution. Our framework could be used to
252 predict radiative imbalance into the future, because surface warming and radiative forcing are – in
253 principle, partially – predictable.

254 **Materials and Methods**

255 *Convolutional neural network*

256 The convolutional neural network (CNN) consists of a series of convolutional, max pooling, and
257 fully connected layers (Supporting Information Fig. 1). The input data (yearly surface temperature
258 maps) is passed through a convolutional layer with 32 kernels of size 3×3 , a max pooling layer
259 with a 2×2 kernel, a second convolutional layer (32 kernels, size 3×3), and another max pooling
260 layer (2×2 kernel). The output from the second max pooling layer is flattened and connected to two
261 fully connected layers, with 32 and 16 nodes, before being compared to the output (global mean
262 radiation). Every layer uses a ELU activation function, except for the last dense layer, which uses a
263 linear one. We have tested different CNN architectures (Supporting Information Fig. 2 and Tab. 1)
264 and chose the setup that performed best (lowest mean squared error) on the testing output data.

265 Because the CNN depicts a nonlinear function, its gradient is state dependent. To compute the
266 gradient map in Fig. 2, derivatives with respect to local temperature are evaluated with the test-
267 ing dataset (internal variability in the climate models, see below) and averaged over all years and
268 ensemble members. Gradient maps averaged over members from individual climate models look
269 similar to the one shown in Fig. 2, indicating that the average gradient in Fig. 2 is a good repre-
270 sentation of all models. We use the CNN trained on four climate models simultaneously, under the
271 assumption that, combined, they display enough variability to encompass observed variations of R
272 with T .

273 *Global climate model data*

274 The CNN is trained on four different large ensemble climate models: CanESM5 (Swart et al.
275 2019), IPSL-CM6A-LR (Boucher et al. 2020), MIROC6 (Tatebe et al. 2019), and MPI-ESM1.1
276 (Maher et al. 2019). These models were selected based on two criteria: (1) they have at least
277 25 ensemble members; and (2) they contributed to the Radiative Forcing Model Intercomparison
278 Project (RFMIP, Pincus et al. 2016), which provides dedicated simulations to quantify the radiative
279 forcing (used as perfect model testbed in Fig. 3 and to compute the internal variability of R for
280 training the CNN).

281 The input training data are maps of annual surface temperature (T). The output training data is
282 global-mean radiation R , computed by subtracting the forcing F from the net radiative imbalance

283 N . We define a downward flux at the top of the atmosphere as positive. The forcing F is com-
284 puted from a dedicated model run and is the same for all ensemble members, but model-dependent
285 (Pincus et al. 2016). N is available as standard model output as the sum of incoming shortwave,
286 outgoing shortwave, and outgoing longwave. CanESM5, IPSL-CM6A-LR, and MIROC6 simulate
287 the historical forcing from 1870-2014 and the Shared Socio-economic Pathway 2-4.5 (SSP2-4.5)
288 for following years. MPI-ESM1.1 simulates historical forcing from 1870-2004 followed by the rep-
289 resentative concentration pathway 8.5 (RCP8.5). We apply a land mask to the surface temperature,
290 such that we can use observed sea surface temperature datasets (see below). However, using a CNN
291 trained on surface temperature over both land and ocean does not significantly alter our results.

292 We use annual means from 1870 to 2039 (the longest period of overlap across the model data)
293 and scale to the resolution of CanESM5 ($\sim 2.8^\circ$) using a bilinear regridder with period boundary
294 conditions. We use 25 ensemble members from each model, of which 19 are used for training, 3 for
295 validation, and 3 for testing. In total, we train on $19 \times 4 = 76$ ensemble members over a period of
296 169 years, evenly distributed over the four models. In order to use a minimal amount of information
297 from climate models, T and R are detrended by removing the ensemble mean (at every grid point,
298 for each model separately), effectively removing the forcing (Suarez-Gutierrez et al. 2021). Hence,
299 any climate change information is removed, except for the indirect effect of the forcing on internal
300 variability. Only this detrended data is used to train the CNN, and thus the CNN has never seen a
301 forced response during training.

302 *Observational data*

303 When estimating the forcing (Fig. 1), we use temperature data from four different observa-
304 tional/reanalysis datasets: the European Centre for Medium-Range Weather Forecasts Reanalysis
305 v5 (ERA5, Hersbach et al. 2020, 2023), COBE2 (Hirahara et al. 2014), NOAAGlobalTemp 6.0.0
306 (Huang et al. 2022, 2024), and The Hadley Centre Global Sea Ice and Sea Surface Temperature
307 (HadISST-1.1, Rayner et al. 2003). All data are interpolated to the same grid as the CNN input data
308 ($\sim 2.8^\circ$) using a bilinear scheme with periodic boundary conditions. Note that NOAAGlobalTemp
309 has a native grid of 5° , and thus had to be downsampled, while the other datasets have a smaller native
310 grid. After regridding, the largest overlap of land areas across datasets is used as a land mask and
311 applied to all training, validation, and testing data.

312 The observational datasets (apart from ERA5) report sea surface temperature (SST), and not
313 near-surface air temperature (TAS), on which the CNN is trained. For ERA5, we compare CNN
314 predictions based on SST and TAS and find similar values of the radiation (Supporting Information
315 Fig. 4a, TAS is used in the main text). The forcing trend predicted from SST is slightly lower than
316 the one predicted from TAS, but is not significantly different (Supporting Information Fig. 4b).

317 For the observed radiative imbalance N , we use satellite observations from CERES-EBAF4.2
318 (Loeb et al. 2018; NASA/LARC/SD/ASDC 2023). Yearly averages from 2001-2023 are computed
319 from monthly data of globally-averaged net top of the atmosphere radiative fluxes. From 1985-
320 2000, we use a reconstruction (DEEP-C, Allan et al. 2014; Liu et al. 2020) based on older satellite
321 observations and model simulations. Note that the reconstruction before 2001 uses models and
322 reanalyses, and is therefore less reliable than the direct observations derived from CERES (Raghu-
323 raman et al. 2019, 2023; Loeb et al. 2024a).

324 *Trend analysis*

325 Trends are calculated from yearly averages using ordinary least squares. We include predictions
326 from all four temperature datasets in the calculation of the overall trend. We compare the overall
327 trend with the trend of individual observational datasets and find similar results (within 5-95%
328 confidence bounds). For the individual datasets, we find a trend in F of $0.69 \pm 0.21 \text{ Wm}^{-2}\text{decade}^{-1}$
329 (ERA5), $0.70 \pm 0.21 \text{ Wm}^{-2}\text{decade}^{-1}$ (COBE2), $0.76 \pm 0.20 \text{ Wm}^{-2}\text{decade}^{-1}$ (NOAAGlobalTemp),
330 and $0.70 \pm 0.19 \text{ Wm}^{-2}\text{decade}^{-1}$ (HadISST-1.1).

331 We estimate the uncertainty in the trend of F by combining the uncertainties in the trends in
332 N and R . Raghuraman et al. (2021) estimated the 95% confidence range of the trend in N to
333 be $0.20 \text{ Wm}^{-2}\text{decade}^{-1}$, which encompasses different observational uncertainties (see also Loeb
334 et al. 2021, 2022; Hodnebrog et al. 2024). Assuming a normal distribution, this converts to a
335 standard error of $\sigma_N = 0.10 \text{ Wm}^{-2}\text{decade}^{-1}$. The standard error of the trend in R is computed
336 for every observational dataset separately, and the mean is taken over all four datasets, that is,
337 $\sigma_R^2 = \sum_{j=1}^5 \sigma_j^2 / 5$. The uncertainty in the trend in R does not include any uncertainty introduced
338 by the CNN. Finally, the standard error of the trend in F is estimated to be $\sigma_F = \sqrt{\sigma_N^2 + \sigma_R^2}$, and
339 converted to a 5-95% confidence range by assuming the trend slope follows a t -distribution with
340 21 degrees of freedom.

341 *Data availability*

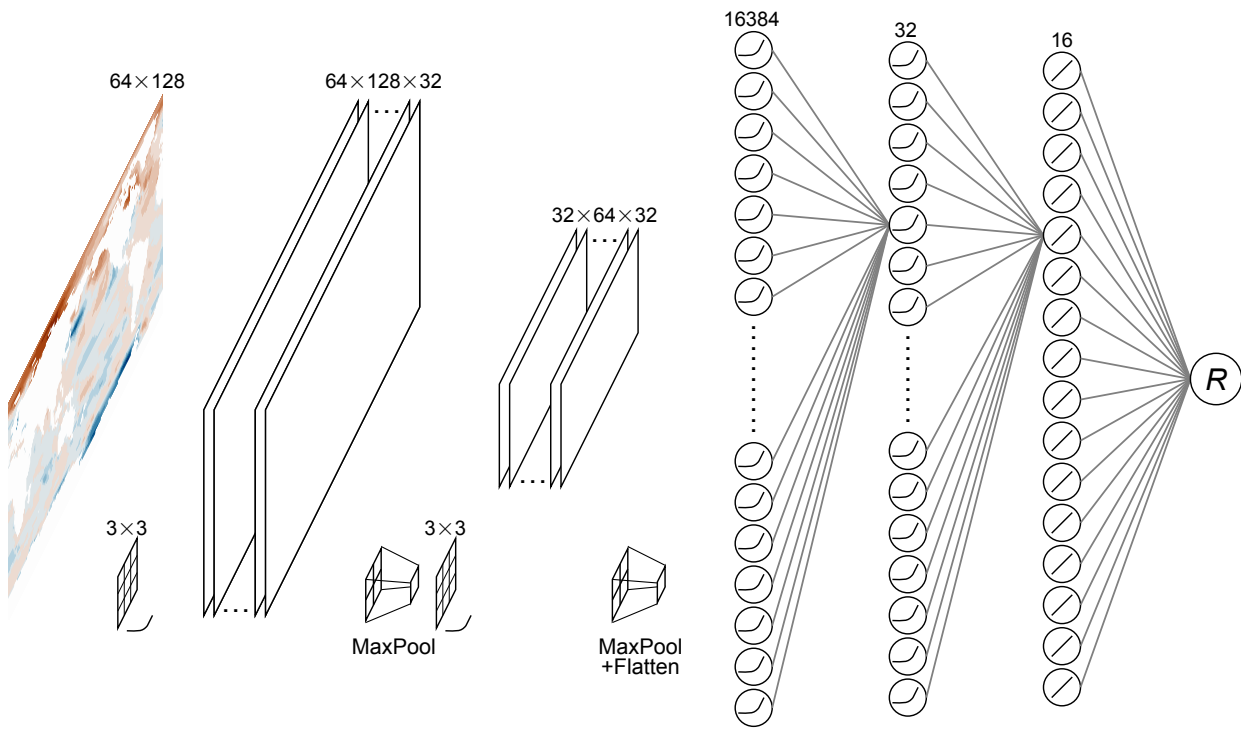
342 All climate model data is standard CMIP model output, and is made freely available by the Earth
343 System Grid Federation (ESGF) at <https://esgf-node.llnl.gov/>. Observational temperature data
344 is available from <https://doi.org/10.24381/cds.adbb2d47> (ERA5), <https://psl.noaa.gov/data/gridded/data.cobe2.html> (COBE2), <https://www.ncei.noaa.gov/products/land-based-station/noaa-global-temp> (NOAAGlobalTemp), and <https://www.metoffice.gov.uk/hadobs/hadisst/> (HadISST-
346 1.1). The observed radiative imbalance can be downloaded at <https://ceres.larc.nasa.gov/data/>
347 (CERES-EBAF4.2) and <https://researchdata.reading.ac.uk/347/> (DEEP-C).
348

349 *Code availability*

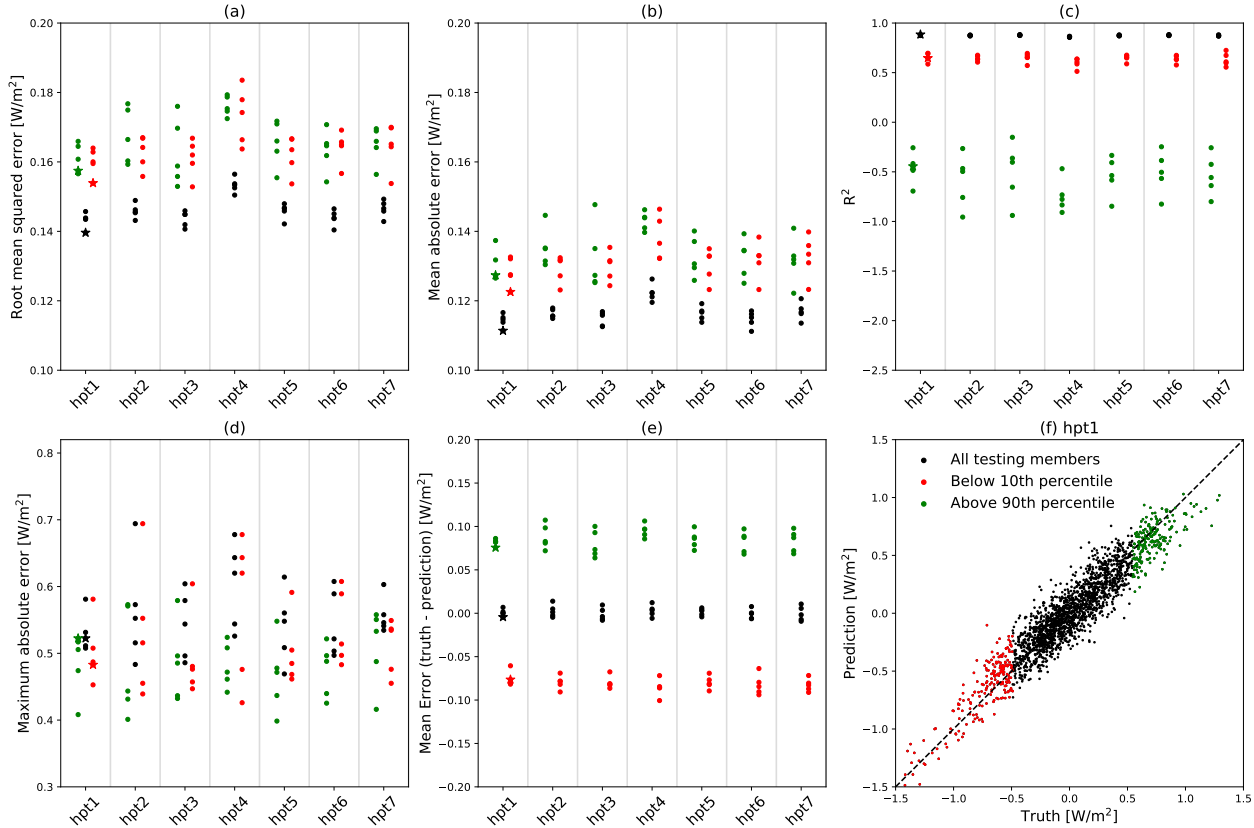
350 All reported results were analyzed using Python-3.10, and the CNNs were trained using
351 Tensorflow-2.15. All code will be made available at the time of acceptance of the manuscript.

352 *Acknowledgements*

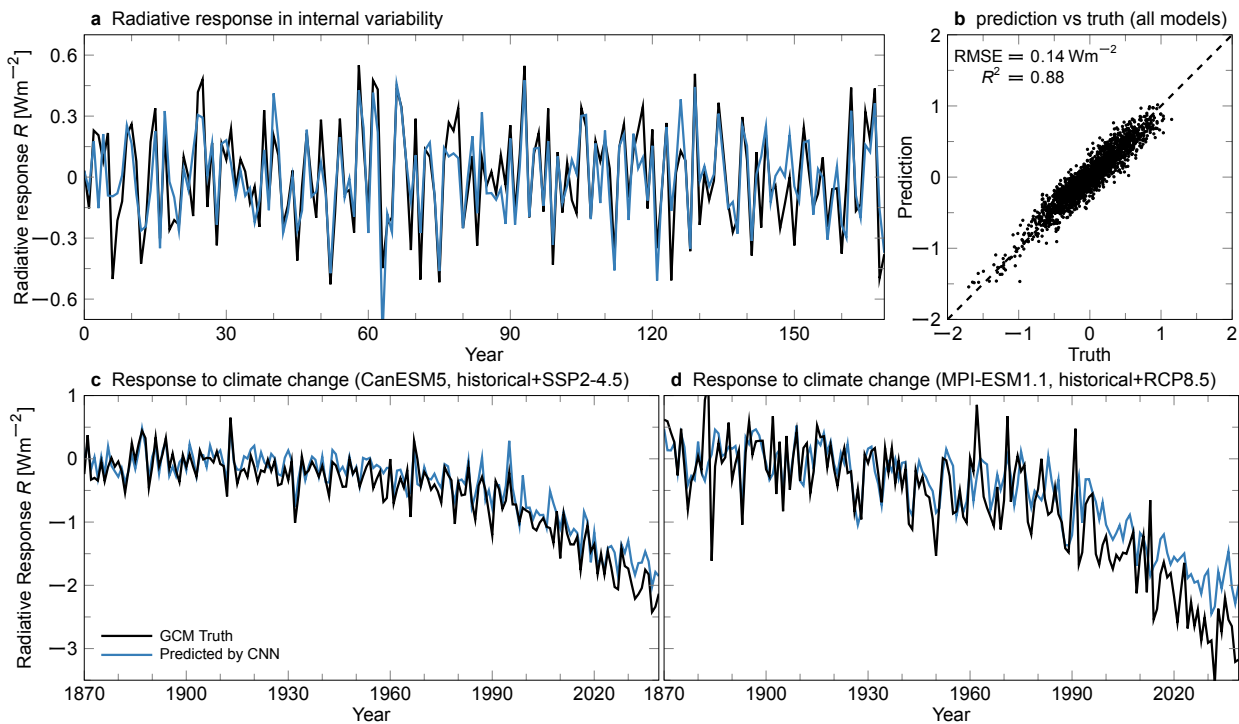
353 We thank Dirk Olonscheck for sharing large-ensemble and forcing climate model data and Mark
354 Zelinka for sharing observational temperature datasets. We thank Marybeth Arcodia, Candace
355 Bethea, Leif Fredericks, Rich Karp, and Shiv Priyam Raghuraman for comments on the manuscript.
356 EAB was supported, in part, by the Regional and Global Model Analysis program area of the U.S.
357 Department of Energy's (DOE) Office of Biological and Environmental Research (BER) as part of
358 the Program for Climate Model Diagnosis and Intercomparison project.



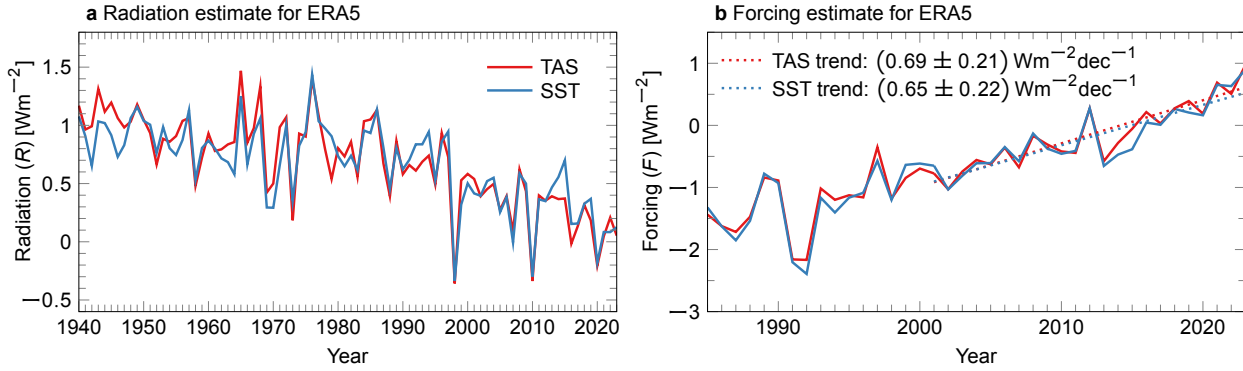
360 **Supporting Information Fig. 1. Schematic of the architecture of the CNN used.** The input maps (surface
 361 temperature) are passed through two convolutional layers, each with 32 kernels of size 3×3 and followed by
 362 a max pooling layer and a ReLu activation function. The result is flattened and passed through two additional
 363 fully connected layers with 32 and 16 neurons, again with a ReLu activation function. The final result is a single
 364 number estimating the global-mean radiative response R .



365 **Supporting Information Fig. 2. Hyperparameter testing for different CNN architectures.** The x -axis
 366 labels are defined in Supporting Information Tab. 1, and each dot represents a different random initialization of
 367 the CNN before training. For each trained CNN, we compute the (a) root mean squared error, (b) mean absolute
 368 error, (c) R^2 value, (d) maximum absolute error, and (e) mean error (truth-prediction). Panel (f) reports the truth
 369 versus prediction of all years in the testing dataset. Black dots represent all years, while red and green dots show
 370 only those in the lower and upper 10th percentiles, to examine how well the CNN performs on the extremes. The
 371 CNN used in the main text is highlighted by a star.



372 **Supporting Information Fig. 3. Verification of the CNN.** Panel (a) shows the truth (black) and predictions
 373 (blue) for a single ensemble member in the testing dataset, for internal variability of the temperature and radiative
 374 response. Panel (b) shows the true versus the predicted radiative response for all years in the testing dataset; the
 375 CNN explains 85% of the variance across all testing members. Panels (c) and (d) show the CNN applied to an
 376 out-of-sample member that experiences forced climate change for two different models used in training. Even
 377 though the CNN has never seen climate change during training, it can predict the response to forcing well.



378 **Supporting Information Fig. 4. Comparison of near-surface temperature (TAS) and sea surface tem-**
 379 **perature (SST) as input for the convolutional neural network.** Panel (a) shows the predicted radiation (R)
 380 and (b) shows the predicted forcing ($F = N - R$). Dotted lines in (b) are forcing trends in 2001-2023. We use
 381 ERA5 data and our CNN from the main text. Both predictions are very similar; therefore, we expect only minor
 382 differences when using observational datasets of SST compared to TAS.

383 **Supporting Information Table 1. Hyperparameters used in testing different CNN architectures in Sup-**
 384 **porting Information Fig. 2.** All CNNs use a similar architecture as shown in Supporting Information Fig. 1,
 385 but we change the number of convolutional layers/kernels, kernel size, and amount of dense layers/nodes. The
 386 set of hyperparameters used in the main text is hpt1.

	Convolutional layers	Kernel size	Dense layers
hpt1	[32, 32]	3×3	[32, 16]
hpt2	[32, 32]	5×5	[32, 16]
hpt3	[64, 64]	3×3	[32, 16]
hpt4	[32, 32, 32]	3×3	[32, 16]
hpt5	[16, 16]	3×3	[32, 16]
hpt6	[32, 32]	3×3	[16, 16]
hpt7	[32, 32]	3×3	[8, 8, 16]

References

- Alessi, M. J., and M. Rugenstein, 2023: Surface Temperature Pattern Scenarios Suggest Higher Warming Rates Than Current Projections. *Geophysical Research Letters*, **50** (23), e2023GL105795, <https://doi.org/10.1029/2023GL105795>.
- Allan, R. P., C. Liu, N. G. Loeb, M. D. Palmer, M. Roberts, D. Smith, and P.-L. Vidale, 2014: Changes in global net radiative imbalance 1985–2012. *Geophysical research letters*, **41** (15), 5588–5597, <https://doi.org/10.1002/2014GL060962>.
- Andrews, T., J. M. Gregory, and M. J. Webb, 2015: The Dependence of Radiative Forcing and Feedback on Evolving Patterns of Surface Temperature Change in Climate Models. *Journal of Climate*, **28** (4), 1630–1648, <https://doi.org/10.1175/JCLI-D-14-00545.1>.
- Bellouin, N., and Coauthors, 2020: Bounding Global Aerosol Radiative Forcing of Climate Change. *Reviews of Geophysics*, **58** (1), e2019RG000660, <https://doi.org/10.1029/2019RG000660>.
- Bloch-Johnson, J., M. Rugenstein, M. B. Stolpe, T. Rohrschneider, Y. Zheng, and J. M. Gregory, 2021: Climate Sensitivity Increases Under Higher CO₂ Levels Due to Feedback Temperature Dependence. *Geophysical Research Letters*, **48** (4), e2020GL089074, <https://doi.org/10.1029/2020GL089074>.
- Boucher, O., and Coauthors, 2020: Presentation and evaluation of the IPSL-CM6A-LR climate model. *Journal of Advances in Modeling Earth Systems*, **12** (7), e2019MS002010, <https://doi.org/10.1029/2019MS002010>.
- Ceppi, P., and P. Nowack, 2021: Observational evidence that cloud feedback amplifies global warming. *Proceedings of the National Academy of Sciences*, **118** (30), <https://doi.org/10.1073/pnas.2026290118>.
- Cess, R. D., and Coauthors, 1990: Intercomparison and interpretation of climate feedback processes in 19 atmospheric general circulation models. *Journal of Geophysical Research: Atmospheres*, **95** (D10), 16601–16615, <https://doi.org/10.1029/JD095iD10p16601>.
- Charney, J., and Coauthors, 1979: Carbon Dioxide and Climate: A Scientific Assessment. Tech. rep., National Academy of Science, Washington, DC. <https://doi.org/10.17226/12181>.
- Cheng, L., K. Von Schuckmann, A. Minière, M. Z. Hakuba, S. Purkey, G. A. Schmidt, and Y. Pan, 2024: Ocean heat content in 2023. *Nature Reviews Earth & Environment*, **5** (4), 232–234, <https://doi.org/10.1038/s43017-024-00539-9>.
- Dessler, A. E., 2010: A Determination of the Cloud Feedback from Climate Variations over the Past Decade. *Science*, **330** (6010), 1523–1527, <https://doi.org/10.1126/science.1192546>.
- Dessler, A. E., and P. M. Forster, 2018: An Estimate of Equilibrium Climate Sensitivity From Interannual Variability. *Journal of Geophysical Research: Atmospheres*, **123** (16), 8634–8645, <https://doi.org/10.1029/2018JD028481>.
- Dong, Y., C. Proistosescu, K. C. Armour, and D. S. Battisti, 2019: Attributing Historical and Future Evolution of Radiative Feedbacks to Regional Warming Patterns using a Green’s Function Approach: The Preeminence of the Western Pacific. *Journal of Climate*, **32** (17), 5471–5491, <https://doi.org/10.1175/JCLI-D-18-0843.1>.

- 427 Esper, J., M. Torbenson, and U. Büntgen, 2024: 2023 summer warmth unparalleled over the past
428 2,000 years. *Nature*, **631 (8019)**, 94–97, <https://doi.org/10.1038/s41586-024-07512-y>.
- 429 Forster, P., and Coauthors, 2021: The Earth’s Energy Budget, Climate Feedbacks, and Climate
430 Sensitivity. *Climate Change 2021: The Physical Science Basis. Contribution of Working Group
431 I to the Sixth Assessment Report of the Intergovernmental Panel on Climate Change*, V. Masson-
432 Delmotte, P. Zhai, A. Pirani, S. L. Connors, C. Péan, S. Berger, N. Caud, Y. Chen, L. Goldfarb,
433 M. I. Gomis, M. Huang, K. Leitzell, E. Lonnoy, J. B. R. Matthews, T. K. Maycock, T. Waterfield,
434 O. Yelekçi, R. Yu, and B. Zhou, Eds., Cambridge University Press, Cambridge, UK and New
435 York, NY, USA, book section 7, 923–1054, <https://doi.org/10.1017/9781009157896.009>.
- 436 Forster, P. M., and Coauthors, 2024: Indicators of Global Climate Change 2023: annual update
437 of key indicators of the state of the climate system and human influence. *Earth System Science
438 Data*, **16 (6)**, 2625–2658, <https://doi.org/10.5194/essd-16-2625-2024>.
- 439 Gettelman, A., and Coauthors, 2024: Has Reducing Ship Emissions Brought Forward Global
440 Warming? *Geophysical Research Letters*, **51 (15)**, e2024GL109077, <https://doi.org/10.1029/2024GL109077>.
- 442 Gregory, J. M., T. Andrews, P. Ceppi, T. Mauritsen, and M. J. Webb, 2020: How accurately can
443 the climate sensitivity to CO₂ be estimated from historical climate change? *Climate Dynamics*,
444 **54 (1)**, 129–157, <https://doi.org/10.1007/s00382-019-04991-y>.
- 445 Gregory, J. M., and Coauthors, 2004: A new method for diagnosing radiative forcing and climate
446 sensitivity. *Geophysical Research Letters*, **31 (3)**, <https://doi.org/10.1029/2003GL018747>.
- 447 Hersbach, H., and Coauthors, 2020: The ERA5 global reanalysis. *Quarterly Journal of the Royal
448 Meteorological Society*, **146 (730)**, 1999–2049, <https://doi.org/10.1002/qj.3803>.
- 449 Hersbach, H., and Coauthors, 2023: ERA5 hourly data on single levels from 1940 to present.
450 Copernicus Climate Change Service (C3S) Climate Data Store (CDS). [https://doi.org/10.24381/](https://doi.org/10.24381/cds.adbb2d47)
451 [cds.adbb2d47](https://doi.org/10.24381/cds.adbb2d47).
- 452 Hirahara, S., M. Ishii, and Y. Fukuda, 2014: Centennial-Scale Sea Surface Temperature
453 Analysis and Its Uncertainty. *Journal of Climate*, **27 (1)**, 57 – 75, [https://doi.org/10.1175/](https://doi.org/10.1175/JCLI-D-12-00837.1)
454 [JCLI-D-12-00837.1](https://doi.org/10.1175/JCLI-D-12-00837.1).
- 455 Hodnebrog, Ø., and Coauthors, 2024: Recent reductions in aerosol emissions have increased
456 Earth’s energy imbalance. *Communications Earth & Environment*, **5 (1)**, 166, [https://doi.org/](https://doi.org/10.1038/s43247-024-01324-8)
457 [10.1038/s43247-024-01324-8](https://doi.org/10.1038/s43247-024-01324-8).
- 458 Huang, B., X. Yin, M. J. Menne, R. Vose, and H.-M. Zhang, 2022: Improvements to the Land
459 Surface Air Temperature Reconstruction in NOAAGlobalTemp: An Artificial Neural Network
460 Approach. *Artificial Intelligence for the Earth Systems*, **1 (4)**, e220032, [https://doi.org/10.1175/](https://doi.org/10.1175/AIES-D-22-0032.1)
461 [AIES-D-22-0032.1](https://doi.org/10.1175/AIES-D-22-0032.1).
- 462 Huang, B., X. Yin, M. J. Menne, R. S. Vose, and H.-M. Zhang, 2024: NOAA Global Surface
463 Temperature Dataset (NOAAGlobalTemp), Version 6.0.0. <https://doi.org/10.25921/rzxcg-p717>.
- 464 Jiang, N., and Coauthors, 2024: Enhanced risk of record-breaking regional temperatures during the
465 2023–24 El Niño. *Scientific Reports*, **14 (1)**, 2521, <https://doi.org/10.1038/s41598-024-52846-2>.

- 466 Knutti, R., and M. A. A. Rugenstein, 2015: Feedbacks, climate sensitivity and the limits of linear
467 models. *Philosophical Transactions of the Royal Society of London A: Mathematical, Physical*
468 *and Engineering Sciences*, **373 (2054)**, <https://doi.org/10.1098/rsta.2015.0146>.
- 469 Kramer, R. J., H. He, B. J. Soden, L. Oreopoulos, G. Myhre, P. M. Forster, and C. J. Smith, 2021:
470 Observational Evidence of Increasing Global Radiative Forcing. *Geophysical Research Letters*,
471 **48 (7)**, e2020GL091585, <https://doi.org/10.1029/2020GL091585>.
- 472 Kuhlbrodt, T., R. Swaminathan, P. Ceppi, and T. Wilder, 2024: A Glimpse into the Future: The
473 2023 Ocean Temperature and Sea Ice Extremes in the Context of Longer-Term Climate Change.
474 *Bulletin of the American Meteorological Society*, **105 (3)**, E474 – E485, [https://doi.org/10.1175/
475 BAMS-D-23-0209.1](https://doi.org/10.1175/BAMS-D-23-0209.1).
- 476 LeCun, Y., Y. Bengio, and G. Hinton, 2015: Deep learning. *Nature*, **521 (7553)**, 436–444,
477 <https://doi.org/10.1038/nature14539>.
- 478 Lee, J.-Y., and Coauthors, 2021: Future Global Climate: Scenario-Based Projections and Near-
479 Term Information. *Climate Change 2021: The Physical Science Basis. Contribution of Working*
480 *Group I to the Sixth Assessment Report of the Intergovernmental Panel on Climate Change*,
481 V. Masson-Delmotte, P. Zhai, A. Pirani, S. L. Connors, C. Péan, S. Berger, N. Caud, Y. Chen,
482 L. Goldfarb, M. I. Gomis, M. Huang, K. Leitzell, E. Lonnoy, J. B. R. Matthews, T. K. Maycock,
483 T. Waterfield, O. Yelekçi, R. Yu, and B. Zhou, Eds., Cambridge University Press, Cambridge,
484 UK and New York, NY, USA, book section 4, 553–672, [https://doi.org/10.1017/9781009157896.
485 006](https://doi.org/10.1017/9781009157896.006).
- 486 Liu, C., and R. Allan, 2022: Reconstructions of the radiation fluxes at the top of atmosphere and
487 net surface energy flux: DEEP-C Version 5.0. University of Reading, URL [https://researchdata.
488 reading.ac.uk/347/](https://researchdata.reading.ac.uk/347/), <https://doi.org/10.1175/JCLI-D-17-0137.1>.
- 489 Liu, C., and Coauthors, 2020: Variability in the global energy budget and transports 1985–2017.
490 *Climate Dynamics*, **55**, 3381–3396, <https://doi.org/10.1007/s00382-020-05451-8>.
- 491 Loeb, N. G., D. R. Doelling, S. Kato, W. Su, P. E. Mlynckzak, and J. C. Wilkins, 2024a: Continuity
492 in Top-of-Atmosphere Earth Radiation Budget Observations. *Journal of Climate*, [https://doi.org/
493 10.1175/JCLI-D-24-0180.1](https://doi.org/10.1175/JCLI-D-24-0180.1).
- 494 Loeb, N. G., S.-H. Ham, R. P. Allan, T. J. Thorsen, B. Meyssignac, S. Kato, G. C. Johnson, and
495 J. M. Lyman, 2024b: Observational Assessment of Changes in Earth’s Energy Imbalance Since
496 2000. *Surveys in Geophysics*, <https://doi.org/10.1007/s10712-024-09838-8>.
- 497 Loeb, N. G., G. C. Johnson, T. J. Thorsen, J. M. Lyman, F. G. Rose, and S. Kato, 2021: Satellite
498 and Ocean Data Reveal Marked Increase in Earth’s Heating Rate. *Geophysical Research Letters*,
499 e2021GL093047, <https://doi.org/10.1029/2021GL093047>.
- 500 Loeb, N. G., and Coauthors, 2018: Clouds and the Earth’s Radiant Energy System (CERES) Energy
501 Balanced and Filled (EBAF) Top-of-Atmosphere (TOA) Edition-4.0 Data Product. *Journal of*
502 *Climate*, **31 (2)**, 895 – 918, <https://doi.org/10.1175/JCLI-D-17-0208.1>.
- 503 Loeb, N. G., and Coauthors, 2022: Evaluating twenty-year trends in Earth’s energy flows
504 from observations and reanalyses. *Journal of Geophysical Research: Atmospheres*, **127 (12)**,
505 e2022JD036686, <https://doi.org/10.1029/2022JD036686>.

- 506 Lutsko, N. J., and K. Takahashi, 2018: What Can the Internal Variability of CMIP5 Models Tell
507 Us about Their Climate Sensitivity? *Journal of Climate*, **31** (13), 5051–5069, [https://doi.org/](https://doi.org/10.1175/JCLI-D-17-0736.1)
508 10.1175/JCLI-D-17-0736.1.
- 509 Maher, N., and Coauthors, 2019: The Max Planck Institute Grand Ensemble: Enabling the Explo-
510 ration of Climate System Variability. *Journal of Advances in Modeling Earth Systems*, **11** (7),
511 2050–2069, <https://doi.org/10.1029/2019MS001639>.
- 512 Maher, N., and Coauthors, 2023: The future of the El Niño–Southern Oscillation: using large
513 ensembles to illuminate time-varying responses and inter-model differences. *Earth System Dy-*
514 *namics*, **14** (2), 413–431, <https://doi.org/10.5194/esd-14-413-2023>.
- 515 Mamalakis, A., E. A. Barnes, and I. Ebert-Uphoff, 2022: Investigating the Fidelity of Ex-
516 plainable Artificial Intelligence Methods for Applications of Convolutional Neural Networks
517 in Geoscience. *Artificial Intelligence for the Earth Systems*, **1** (4), e220012, [https://doi.org/](https://doi.org/10.1175/AIES-D-22-0012.1)
518 10.1175/AIES-D-22-0012.1.
- 519 Min, S.-K., 2024: Human influence can explain the widespread exceptional warmth in 2023. *Com-*
520 *munications Earth & Environment*, **5** (1), 215, <https://doi.org/10.1038/s43247-024-01391-x>.
- 521 Minnis, P., E. F. Harrison, L. L. Stowe, G. Gibson, F. M. Denn, D. Doelling, and W. Smith Jr, 1993:
522 Radiative climate forcing by the Mount Pinatubo eruption. *Science*, **259** (5100), 1411–1415,
523 <https://doi.org/10.1126/science.259.5100.1411>.
- 524 Myers, T. A., R. C. Scott, M. D. Zelinka, S. A. Klein, J. R. Norris, and P. M. Caldwell, 2021:
525 Observational constraints on low cloud feedback reduce uncertainty of climate sensitivity. *Nature*
526 *Climate Change*, **11** (6), 501–507, <https://doi.org/10.1038/s41558-021-01039-0>.
- 527 NASA/LARC/SD/ASDC, 2023: CERES Energy Balanced and Filled (EBAF) TOA and Surface
528 Monthly means data in netCDF Edition 4.2. NASA Langley Atmospheric Science Data Center
529 DAAC, https://doi.org/10.5067/TERRA-AQUA-NOAA20/CERES/EBAF_L3B004.2.
- 530 Olonscheck, D., and M. Rugenstein, 2024: Coupled Climate Models Systematically Under-
531 estimate Radiation Response to Surface Warming. *Geophysical Research Letters*, **51** (6),
532 e2023GL106909, <https://doi.org/10.1029/2023GL106909>.
- 533 Pincus, R., P. M. Forster, and B. Stevens, 2016: The Radiative Forcing Model Intercomparison
534 Project (RFMIP): experimental protocol for CMIP6. *Geoscientific Model Development*, **9** (9),
535 3447–3460, <https://doi.org/10.5194/gmd-9-3447-2016>.
- 536 Quaas, J., and Coauthors, 2022: Robust evidence for reversal of the trend in aerosol effective
537 climate forcing. *Atmospheric Chemistry and Physics*, **22** (18), 12 221–12 239, [https://doi.org/](https://doi.org/10.5194/acp-22-12221-2022)
538 10.5194/acp-22-12221-2022.
- 539 Raghuraman, S. P., D. Paynter, R. Menzel, and V. Ramaswamy, 2023: Forcing, Cloud Feedbacks,
540 Cloud Masking, and Internal Variability in the Cloud Radiative Effect Satellite Record. *Journal*
541 *of Climate*, **36** (12), 4151 – 4167, <https://doi.org/10.1175/JCLI-D-22-0555.1>.
- 542 Raghuraman, S. P., D. Paynter, and V. Ramaswamy, 2019: Quantifying the Drivers of the Clear
543 Sky Greenhouse Effect, 2000-2016. *Journal of Geophysical Research: Atmospheres*, **124** (21),
544 11 354–11 371, <https://doi.org/10.1029/2019JD031017>.

- 545 Raghuraman, S. P., D. Paynter, and V. Ramaswamy, 2021: Anthropogenic forcing and response
546 yield observed positive trend in Earth's energy imbalance. *Nature Communications*, **12** (1), 4577,
547 <https://doi.org/10.1038/s41467-021-24544-4>.
- 548 Raghuraman, S. P., B. Soden, A. Clement, G. Vecchi, S. Menemenlis, and W. Yang, 2024: The 2023
549 global warming spike was driven by the El Niño–Southern Oscillation. *Atmospheric Chemistry
550 and Physics*, **24** (19), 11 275–11 283, <https://doi.org/10.5194/acp-24-11275-2024>.
- 551 Rantanen, M., and A. Laaksonen, 2024: The jump in global temperatures in September 2023 is ex-
552 tremely unlikely due to internal climate variability alone. *npj Climate and Atmospheric Science*,
553 **7** (1), 34, <https://doi.org/10.1038/s41612-024-00582-9>.
- 554 Rayner, N. A., D. E. Parker, E. B. Horton, C. K. Folland, L. V. Alexander, D. P. Rowell, E. C. Kent,
555 and A. Kaplan, 2003: Global analyses of sea surface temperature, sea ice, and night marine air
556 temperature since the late nineteenth century. *Journal of Geophysical Research: Atmospheres*,
557 **108** (D14), <https://doi.org/10.1029/2002JD002670>.
- 558 Reichstein, M., G. Camps-Valls, B. Stevens, M. Jung, J. Denzler, N. Carvalhais, and Prabhat,
559 2019: Deep learning and process understanding for data-driven Earth system science. *Nature*,
560 **566** (7743), 195–204, <https://doi.org/10.1038/s41586-019-0912-1>.
- 561 Roe, G., 2009: Feedbacks, Timescales, and Seeing Red. *Annual Review of Earth and Planetary
562 Sciences*, **37** (1), 93–115, <https://doi.org/10.1146/annurev.earth.061008.134734>.
- 563 Rugenstein, M., S. Van Loon, and E. A. Barnes, in review: Convolutional neural networks trained
564 on internal variability predict forced response of TOA radiation by learning the pattern effect.
565 *Geophys. Res. Lett.*
- 566 Rugenstein, M., M. Zelinka, K. B. Karaukas, P. Ceppi, and T. Andrews, 2023: Patterns of Surface
567 Warming Matter for Climate Sensitivity. *Eos*, **104**, <https://doi.org/10.1029/2023EO230411>.
- 568 Samset, B. H., M. T. Lund, J. S. Fuglestedt, and L. J. Wilcox, 2024: 2023 temperatures reflect
569 steady global warming and internal sea surface temperature variability. *Communications Earth
570 & Environment*, **5** (1), 460, <https://doi.org/10.1038/s43247-024-01637-8>.
- 571 Schoeberl, M. R., Y. Wang, G. Taha, D. J. Zawada, R. Ueyama, and A. Dessler, 2024: Evolution
572 of the Climate Forcing During the Two Years after the Hunga Tonga-Hunga Ha'apai Eruption.
573 *ESS Open Archive*, <https://doi.org/10.22541/essoar.171255733.32358374/v1>.
- 574 Senior, C. A., and J. F. B. Mitchell, 2000: The time-dependence of climate sensitivity. *Geophysical
575 Research Letters*, **27** (17), 2685–2688, <https://doi.org/10.1029/2000GL011373>.
- 576 Sherwood, S. C., S. Bony, O. Boucher, C. Bretherton, P. M. Forster, J. M. Gregory, and B. Stevens,
577 2015: Adjustments in the Forcing-Feedback Framework for Understanding Climate Change.
578 *Bulletin of the American Meteorological Society*, **96** (2), 217 – 228, [https://doi.org/10.1175/
579 BAMS-D-13-00167.1](https://doi.org/10.1175/BAMS-D-13-00167.1).
- 580 Sherwood, S. C., and Coauthors, 2020: An Assessment of Earth's Climate Sensitivity Using Mul-
581 tiple Lines of Evidence. *Reviews of Geophysics*, **58** (4), <https://doi.org/10.1029/2019RG000678>.
- 582 Smith, C. J., and Coauthors, 2020: Effective radiative forcing and adjustments in CMIP6
583 models. *Atmospheric Chemistry and Physics*, **20** (16), 9591–9618, [https://doi.org/10.5194/
584 acp-20-9591-2020](https://doi.org/10.5194/acp-20-9591-2020).

- 585 Soden, B. J., W. D. Collins, and D. R. Feldman, 2018: Reducing uncertainties in climate models.
586 *Science*, **361 (6400)**, 326–327, <https://doi.org/10.1126/science.aau1864>.
- 587 Stenchikov, G., T. L. Delworth, V. Ramaswamy, R. J. Stouffer, A. Wittenberg, and F. Zeng,
588 2009: Volcanic signals in oceans. *Journal of Geophysical Research: Atmospheres*, **114 (D16)**,
589 <https://doi.org/10.1029/2008JD011673>.
- 590 Storto, A., and C. Yang, 2024: Acceleration of the ocean warming from 1961 to 2022 un-
591 veiled by large-ensemble reanalyses. *Nature Communications*, **15 (1)**, 545, <https://doi.org/10.1038/s41467-024-44749-7>.
- 593 Suarez-Gutierrez, L., S. Milinski, and N. Maher, 2021: Exploiting large ensembles for a better
594 yet simpler climate model evaluation. *Climate Dynamics*, **57 (9)**, 2557–2580, <https://doi.org/10.1007/s00382-021-05821-w>.
- 596 Swart, N. C., and Coauthors, 2019: The Canadian earth system model version 5
597 (CanESM5. 0.3). *Geoscientific Model Development*, **12 (11)**, 4823–4873, <https://doi.org/10.5194/gmd-12-4823-2019>.
- 599 Tatebe, H., and Coauthors, 2019: Description and basic evaluation of simulated mean state, inter-
600 nal variability, and climate sensitivity in MIROC6. *Geoscientific Model Development*, **12 (7)**,
601 2727–2765, <https://doi.org/10.5194/gmd-12-2727-2019>.
- 602 von Schuckmann, K., and Coauthors, 2023: Heat stored in the Earth system 1960–2020: where
603 does the energy go? *Earth System Science Data*, **15 (4)**, 1675–1709, <https://doi.org/10.5194/essd-15-1675-2023>.
- 605 Wood, R., and C. S. Bretherton, 2006: On the Relationship between Stratiform Low Cloud Cover
606 and Lower-Tropospheric Stability. *Journal of Climate*, **19 (24)**, 6425 – 6432, <https://doi.org/10.1175/JCLI3988.1>.
- 608 Yuan, T., and Coauthors, 2024: Abrupt reduction in shipping emission as an inadvertent geoengi-
609 neering termination shock produces substantial radiative warming. *Communications Earth &*
610 *Environment*, **5 (1)**, 281, <https://doi.org/10.1038/s43247-024-01442-3>.